Article

Synthesis and Characterization of Highly Luminescent CdSe–Core CdS/Zn′CdS/ZnS Multishell Nanocrystals

Renguo Xie, Ute Kolb, Jixue Li, Thomas Basch, and Alf Mews

J. Am. Chem. Soc., **2005**, 127 (20), 7480-7488• DOI: 10.1021/ja042939g • Publication Date (Web): 29 April 2005

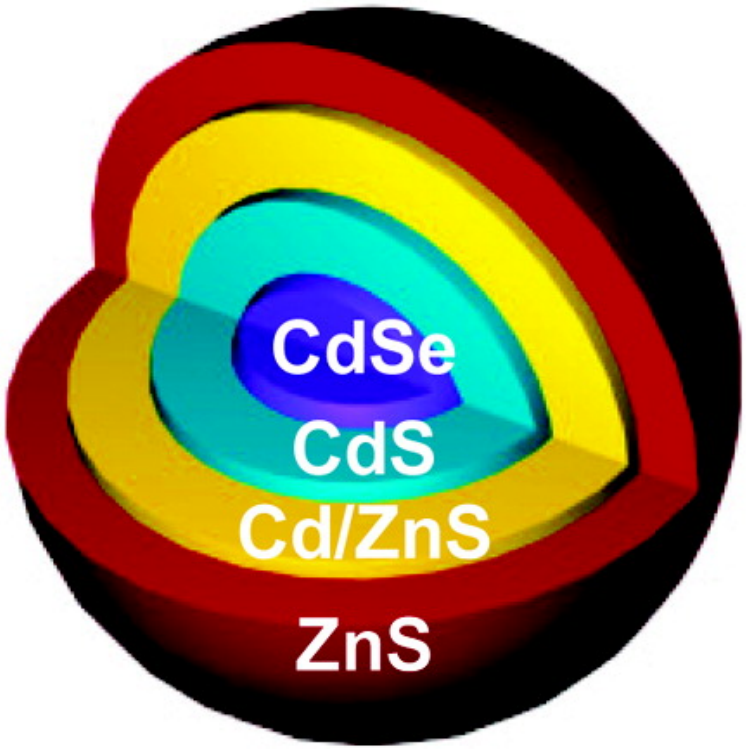

J|A|C|S
ARTICLES
Published on Web 04/29/2005

Synthesis and Characterization of Highly Luminescent CdSe−Core $CdS/Zn_{0.5}Cd_{0.5}S/ZnS$ Multishell Nanocrystals

Renguo Xie, Ute Kolb, Jixue Li, Thomas Basché, and Alf Mews*,†

Contribution from the Institute of Physical Chemistry, University of Mainz, Welderweg 11, 55099 Mainz, Germany

Received November 23, 2004; E-mail: alf.mews@uni-siegen.de

Abstract: We report on the preparation and structural characterization of CdSe nanocrystals, which are covered by a multishell structure from CdS and ZnS. By using the newly developed successive ion layer adhesion and reaction (SILAR) technique, we could gradually change the shell composition from CdS to ZnS in the radial direction. Because of the stepwise adjustment of the lattice parameters in the radial direction, the resulting nanocrystals show a high crystallinity and are almost perfectly spherical, as was investigated by X-ray diffraction and electron microscopy. Also, due to the radial increase of the respective valence- and conduction-band offsets, the nanocrystals are well electronically passivated. This leads to a high fluorescence quantum yield of 70−85% for the amine terminated multishell particles in organic solvents and a quantum yield of up to 50% for mercapto propionic acid-covered particles in water. Finally, we present experimental results that substantiate the superior photochemical and colloidal stability of the multishell particles.

Introduction

Colloidal semiconductor nanocrystals (NCs) are of great interest for both fundamental studies[1−4] and technical applications such as light-emitting devices,[5−8] lasers,[9−11] and fluorescent labels.[12−14] Because of their size-dependent photoluminescence tunable across the visible spectrum,[15] CdSe nanocrystals have become the most extensively investigated NCs. Besides the development of synthesis techniques to prepare samples with narrow size distributions,[16,17] much experimental work is devoted to molecular surface modification to improve the luminescence efficiency[18,19] and colloidal stability of the particles or to develop a reliable processing chemistry.[20,21] However, it is generally difficult to simultaneously passivate both anionic and cationic surface sites by organic ligands. Therefore, dangling bonds will to some extent remain on the surface.[22] To mediate this problem, several methods of inorganic surface modification have been developed to completely passivate the NCs.[23,24] In particular, for CdSe−NCs the particles were covered either with CdS[25] or with ZnS[26] to establish a core/shell system, where the band gap of the core lies energetically within the band gap of the shell material and the photogenerated electrons and holes are mainly confined inside the CdSe. These core/shell NCs have been shown to be generally more robust against chemical degradation or photo-oxidation.[25]

Basically, there are different requirements to form "ideal" core/shell NCs both from a crystallographic and from an electronic point of view. First, to produce particles with high crystallinity, the core and shell materials should have similar lattice parameters such that the shell-growth happens in an epitaxial manner,[25] without the formation of structural defects.

† Current address: Institute of Physical Chemistry, University of Siegen, Adolf-Reichwein-Strasse 2, D-57068 Siegen, Germany.

(1) Brus, L. *J. Phys. Chem.* **1986**, *90*, 2555−2560.
(2) Weller, H. *Angew. Chem.* **1993**, *105*, 43−55.
(3) Greenham, N. C.; Peng, X.; Alivisatos, A. P. *Phys. Rev. B* **1996**, *54*, 17628−17637.
(4) Heath, J. R. *Acc. Chem. Res.* **1999**, *32*, 389−414.
(5) Colvin, V. L.; Schlamp, M. C.; Alivisatos, A. P. *Nature* **1994**, *370*, 354−357.
(6) Coe, S.; Woo, W. K.; Bawendi, M.; Bulovic, V. *Nature* **2002**, *420*, 800−803.
(7) Tessler, N.; Medvedev, V.; Kazes, M.; Kan, S. H.; Banin, U. *Science* **2002**, *295*, 1506−1508.
(8) Hikmet, R. A. M.; Talapin, D. V.; Weller, H. *J. Appl. Phys.* **2003**, *93*, 3509−3514.
(9) Klimov, V. I.; Mikhailovsky, A. A.; Xu, S.; Malko, A.; Hollingsworth, J. A.; Leatherdale, C. A.; Eisler, H. J.; Bawendi, M. G. *Science* **2000**, *290*, 314−317.
(10) Finlayson, C. E.; Russell, D. M.; Ramsdale, C. M.; Ginger, D. S.; Silva, C.; Greenham, N. C. *Adv. Funct. Mater.* **2002**, *12*, 537−540.
(11) Kazes, M.; Lewis, D. Y.; Ebenstein, Y.; Mokari, T.; Banin, U. *Adv. Mater.* **2002**, *14*, 317.
(12) Bruchez, M.; Moronne, M.; Gin, P.; Weiss, S.; Alivisatos, A. P. *Science* **1998**, *281*, 2013−2016.
(13) Chan, W. C. W.; Nie, S. M. *Science* **1998**, *281*, 2016−2018.
(14) Clapp, A. R.; Medintz, I. L.; Mauro, J. M.; Fisher, B. R.; Bawendi, M. G.; Mattoussi, H. *J. Am. Chem. Soc.* **2004**, *126*, 301−310.
(15) Bawendi, M. G.; Carroll, P. J.; Wilson, W. L.; Brus, L. E. *J. Chem. Phys.* **1992**, *96*, 946−954.
(16) Murray, C. B. N., D. J.; Bawendi, M. G. *J. Am. Chem. Soc.* **1993**, *115*, 8706−8715.
(17) Peng, Z. A.; Peng, X. G. *J. Am. Chem. Soc.* **2001**, *123*, 183−184.
(18) Spanhel, L.; Haase, M.; Weller, H.; Henglein, A. *J. Am. Chem. Soc.* **1987**, *109*, 5649−5655.
(19) Talapin, D. V.; Rogach, A. L.; Kornowski, A.; Haase, M.; Weller, H. *Nano Lett.* **2001**, *1*, 207−211.
(20) Wang, Y. A.; Li, J. J.; Chen, H. Y.; Peng, X. G. *J. Am. Chem. Soc.* **2002**, *124*, 2293−2298.
(21) Aldana, J.; Wang, Y. A.; Peng, X. G. *J. Am. Chem. Soc.* **2001**, *123*, 8844−8850.
(22) Katari, J. E. B.; Colvin, V. L.; Alivisatos, A. P. *J. Phys. Chem.* **1994**, *98*, 4109−4117.
(23) Kortan, A. R.; Hull, R.; Opila, R. L.; Bawendi, M. G.; Steigerwald, M. L.; Caroll, R. J.; Brus, L. E. *J. Am. Chem. Soc.* **1990**, *112*, 1327−2332.
(24) Mews, A.; Eychmuller, A.; Giersig, M.; Schooss, D.; Weller, H. *J. Phys. Chem.* **1994**, *98*, 934−941.
(25) Peng, X. G.; Schlamp, M. C.; Kadavanich, A. V.; Alivisatos, A. P. *J. Am. Chem. Soc.* **1997**, *119*, 7019−7029.
(26) Hines, M. A.; Guyot-Sionnest, P. *J. Phys. Chem.* **1996**, *100*, 468−471.

10.1021/ja042939g CCC: $30.25

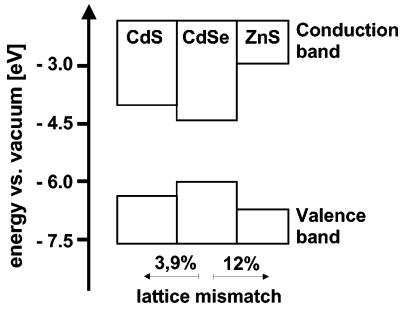

Figure 1. Energetic band positions and lattice mismatch of semiconductor material combinations used in this work.

Second, the shell material should possess a much higher band gap than the core to suppress tunneling of the charge carriers from the cores to the newly formed surface atoms of the shell.[27] Both requirements are not fulfilled for the CdSe/CdS- and CdSe/ZnS-combinations at the same time, because the former material combination has similar lattice parameters but small band-offsets, while the situation is reversed for the latter one. This can be explained by the fact that the band-gap in II−VI-semiconductors is given by ionic and covalent contributions. Essentially, in purely ionic solids (e.g., NaCl), the valence and conduction bands are built up by the anions and cations, respectively. Here, the band gap of ionic solids is larger for materials with higher ionicity, because the different electronegativities lead to a higher separation of the bands.[28] On the other hand, in covalent solids (e.g., Si), the valence and conduction bands are formed by the bonding and antibonding orbitals, respectively. In this case, the band gap is higher at smaller interatomic distances, because the increased spatial overlap between the orbitals leads to a stronger electronic interaction and hence a larger HOMO−LUMO gap.[29]

Because the ionic character within the shell materials CdS and ZnS is similar,[29] the higher band gap in ZnS can be attributed to the smaller interatomic distance with respect to CdS. In Figure 1, we compare the resulting lattice mismatches for the core/shell NCs CdSe/ZnS and CdSe/CdS. It can be seen that the band offsets for the most commonly used core/shell CdSe/ZnS[27] nanocrystals are as high as 0.6 eV for the valence band and 1.44 eV for the conduction band,[30] which leads to an appreciable electronic passivation. On the other hand, the lattice mismatch between CdSe and ZnS is of the order of 12%. Because of this large mismatch, the interface strain accumulates dramatically with increasing shell thickness, and eventually can be released through the formation of misfit dislocations, degrading the optical properties of the NCs. Therefore, for CdSe/ZnS particles prepared by using the "traditional method"[26] (dimethyl zinc and trismethylsilane sulfide), the fluorescence quantum yield is increasing upon growth of the first two monolayers, after which it slowly decreases. This is most likely due to the fact that the lattice defects can act as trapping sites for the photogenerated charge carriers. Another effect of the lattice mismatch is the formation of particles with irregular shape and a broad size distribution upon increasing ZnS-shell thickness.[27]

For the material combination of CdSe-cores and CdS-shells, the interatomic distances are more similar and the lattice mismatch is only 3.9%, which favors the epitaxial growth.[25] On the other hand, the lower band offsets with respect to the ZnS (see Figure 1) hamper the electronic passivation. This point of view is supported by calculations, which showed that especially the wave functions of the electrons extend well across the shell and hence the fluorescence quantum yield is sensitive to surface effects.[25] In addition, it was shown that the high fluorescence quantum yields of up to 80% could only be achieved when the particles were covered with amine ligands, which bind to the surface cadmium atoms and eliminate the electron traps.[25]

To combine the advantages of both shell materials, several methods have been proposed[31] and even implemented[32] to cover nanocrystals or nanorods with a combination of CdS and ZnS. In this work, we present a systematic study where the composition of the shell is gradually changed from CdS to ZnS in the radial direction with atomic precision. This is possible by applying the newly developed SILAR (successive ion layer adsorption and reaction) method from the group of Peng et al., by which layers of different semiconductor materials can be grown successively around the NCs.[33,34] We could reproduce their results and used that method to prepare a new kind of CdSe-NC with a sandwich shell-structure consisting of 2 monolayers (MLs) CdS followed by 3.5 MLs $Zn_{0.5}Cd_{0.5}S$ and finally 2 MLs ZnS as the outermost shell. The $Zn_{0.5}Cd_{0.5}S$ is used as a buffer layer because the band gap as well as the lattice parameters can in principle be adjusted by the composition of alloyed materials, as has been shown recently for $Zn_xCd_{1-x}S$ nanocrystals.[35] For comparison, we also synthesized core/shell particles using the "traditional method[25,27] as well as different particles with the same overall shell thickness of CdS, ZnS, or $Zn_xCd_{1-x}S$ using the SILAR method. The various nanocrystals are compared in terms of crystallinity, size distribution, fluorescence quantum yield, and chemical stability. As precursor materials we exclusively used metal oxides (ZnO and CdO), elementary selenium, and sulfur to completely avoid expensive and hazardous compounds.

Experimental Section

Chemicals. Cadmium oxide (99.99%), sulfur (99.98%, powder), tributylphosphine oxide (TOPO, 90%), zinc oxide (99.99% powder), 1-octadecene (ODE, 90%), oleic acid (OA, 90%), hexamethyldisilathiane ($(TMS)_2S$), tributylphosphine (TBP), mercaptopropionic acid (MPA), and octadecylamine (ODA) were purchased from Aldrich, diethylzinc ($ZnEt_2$) was from Strem Chemicals, and selenium powder (99.5%, 100 mesh) was from Alfa. Tetradecylphosphonic acid (TDPA) was prepared according to the literature.[36]

(27) Dabbousi, B. O.; RodriguezViejo, J.; Mikulec, F. V.; Heine, J. R.; Mattoussi, H.; Ober, R.; Jensen, K. F.; Bawendi, M. G. *J. Phys. Chem. B* **1997**, *101*, 9463−9475.
(28) Phillips, J. C. *Rev. Mod. Phys.* **1997**, *42*, 317−356.
(29) Phillips, J. C.; Van Vechten, J. A. *Phys. Rev. Lett.* **1969**, *22*, 705−708.
(30) Kim, B. S.; Islam, M. A.; Brus, L. E.; Herman, I. P. *J. Appl. Phys.* **2001**, *89*, 8127−8140.
(31) Mekis, I.; Talapin, D. V.; Kornowski, A.; Haase, M.; Weller, H. *J. Phys. Chem. B* **2003**, *107*, 7454−7462.
(32) Manna, L.; Scher, E. C.; Li, L. S.; Alivisatos, A. P. *J. Am. Chem. Soc.* **2002**, *124*, 7136−7145.
(33) Li, J. J.; Wang, Y. A.; Guo, W. Z.; Keay, J. C.; Mishima, T. D.; Johnson, M. B.; Peng, X. G. *J. Am. Chem. Soc.* **2003**, *125*, 12567−12575.
(34) Battaglia, D.; Li, J. J.; Wang, Y. J.; Peng, X. G. *Angew. Chem., Int. Ed.* **2003**, *42*, 5035−5039.
(35) Zhong, X. H.; Feng, Y. Y.; Knoll, W.; Han, M. Y. *J. Am. Chem. Soc.* **2003**, *125*, 13559−13563.
(36) Wu, S. Y.; Casida, J. E. *PSSLEC* **1995**, *102*, 177−184.

Synthesis of CdSe Core NCs. TOPO (or TOPO/ODA)-capped CdSe nanocrystals were synthesized using standard methods.[21] For a typical reaction, a mixture of 0.0514 g of CdO powder, 0.224 g of TDPA, and 4.0 g of TOPO (or 4.0 g of TOPO/ODA-mixture) in a 50 mL three-neck flask was evacuated for 1 h and heated to 320 °C under Ar-flow to form an optically clear solution. The temperature was then lowered to 270 °C, and a solution containing 0.0632 g of Se dissolved in 2.0 g of TBP was injected into the reaction flask. After the injection, the temperature was adjusted to 250 °C for 1 min. After this time, the heating mantle was removed and about 15 mL of methanol was injected at a temperature of 100 °C leading to a precipitation of the nanocrystals. After centrifugation and decantation, the particles were dispersed in chloroform or toluene for further processing. The procedure typically generates CdSe nanocrystals with the first absorption peak around 550 nm, that is, with a diameter of about 3.8 nm.

Synthesis of CdSe/ZnS Core/Shell NCs Using the "Traditional" Method. The ZnS shell growth using the "traditional method" was performed as described previously.[27] In a typical synthesis, a flask containing 5.0 g of TOPO was heated to 100 °C under vacuum for 1 h and then cooled to 60 °C. A defined amount of CdSe NCs[37,38] dispersed in toluene was transferred into the reaction vessel via syringe, and the toluene was pumped off under vacuum. The solution was heated to the desired temperature (135−230 °C), at which a calculated amount of $ZnEt_2$ and $(TMS)_2S$ dissolved in TBP was added dropwise into the vigorously stirred reaction mixture during a period of 5−10 min. This stock solution should be handled with care because of the toxicity of $ZnEt_2$ and the peculiar stench of the $(TMS)_2S$. After the addition was complete, the mixture was cooled to 100 °C and left stirring for 2 h. Finally, the CdSe/ZnS-core/shell NCs were precipitated by addition of methanol, separated, and redispersed for further processing.

Preparation of the Precursor Solution for the SILAR Method. For shell growth using the SILAR method,[33] we used precursor solutions containing only metal oxides (CdO and ZnO), elemental sulfur, and selenium. The zinc precursor solution (0.1 M) was prepared by dissolving ZnO (0.2034 g) in oleic acid (6.18 g) and ODE (18.0 mL) at 310 °C. The cadmium precursor solution (0.1 M) was prepared by dissolving CdO (0.3204 g) in oleic acid (6.18 g) and ODE (18.0 mL) at 240 °C. The Zn/Cd = 1/1 precursor solution (0.1 M) was prepared by dissolving ZnO (0.1017 g) as well as CdO (0.1602 g) in oleic acid (6.18 g) and ODE (18.0 mL) at 300 °C. The sulfur precursor solution (0.1 M) was prepared by dissolving sulfur in ODE at 180 °C. All of the solutions were freshly prepared under Ar-atmosphere. The Cd-, Zn-, and Cd/Zn-precursor solutions were kept at about 80 °C, while the sulfur injection solution was allowed to cool to room temperature. For each shell growth, a calculated amount of a given precursor solution was injected with a syringe using standard air-free procedures.

Calculations of the Amount of Precursor Solutions for Shell Growth. The growth of core/shell nanocrystals using the SILAR method is based on alternating injections of the Zn/Cd- and S-precursors into the solution containing the CdSe-core NCs. The concentration of CdSe-core NCs can be estimated on the basis of the UV−vis spectra.[37,38] The amount of the injection solution for each monolayer can be deduced from a calculation of the number of surface atoms. In this paper, the average thicknesses of one CdS-ML (0.35 nm) and one ZnS-ML (0.31 nm) are estimated on the basis of the wurzite structure of the respective compounds. Hence, the thickness of one monolayer of the alloyed shell ($Zn_{0.5}Cd_{0.5}S$) is assumed to be 0.33 nm, which is consistent with reports from the literature.[35,39]

Preparation of the Core/Shell Nanocrystals Using the SILAR Technique. The SILAR technique allows for growing complex shells around a given CdSe-core particle.[33] After slightly changing the reaction conditions reported by Li et al.,[33] we synthesized CdSe/ZnS, CdSe/CdS, CdSe/$Zn_{0.5}Cd_{0.5}S$, and CdSe/CdS/$Zn_{0.5}Cd_{0.5}S$/ZnS with a similar diameter from the same CdSe-core particles. A typical SILAR synthesis was performed as follows: 3 mL of ODE and 1 g of ODA were loaded into a 50 mL reaction vessel, heated to 100 °C under vacuum for 1 h, and cooled to room temperature. The CdSe-NCs in hexane (3.6 nm in diameter, 1.83×10^{-7} mol) were added, and the system was kept at 100 °C under vacuum for 30 min to remove the hexane and other undesired materials of low vapor pressure. Subsequently, the solution was heated to 235 °C under Ar-flow where the shell growth was performed. The choice of this growth temperature was the result of an optimization procedure (200−260 °C) where the optimization parameter was the fluorescence quantum yield of the CdSe/ZnS core/shell particles after shell growth. To calculate the amount of Cd-precursor for the growth of the first monolayer, we assumed that the surface of the CdSe-cores consists equally of Se- and Cd-atoms and therefore used only 50% of the amount of calculated Cd-precursor for a complete ML. Hence, for the "first injection", we used only 0.19 mL instead of 0.37 mL of the Cd-precursor solution. This is followed by alternating addition of Zn-, Cd-, or Zn/Cd-precursors and sulfur precursors, respectively, the amount of which was calculated from the respective volumes of concentric spherical shells with a thickness of one hypothetical monolayer. We found that a period of 10 min between each addition was sufficient for the reaction to be completed, because the UV−vis and PL-spectra showed no further changes after this time period. The complete coverage procedure of CdSe cores with 2 MLs of CdS, 3.5 MLs of $Zn_{0.5}Cd_{0.5}S$, and 2 MLs of ZnS took about 3 h in total. After this time, the solution was kept for another 30 min at 260 °C and finally cooled to room temperature. For purification, 10 mL of hexane was added and the unreacted compounds and byproducts were removed by successive methanol extraction[34] (at least three times) until the methanol phase was clear.

Preparation of the Water-Soluble Nanocrystals. The MPA-coated nanocrystals were synthesized by the phase transfer method[13] in the following manner. The ODA-coated nanocrystals were dissolved in about 2 mL of chloroform to give a high concentration solution (optical density ≈ 2) and added under vigorous stirring to the same volume of a water solution containing MPA. The amount of MPA was adjusted to roughly 150% of the total Cd- or Zn-atoms on the particle surface. After 2 h, the NCs transferred into the water phase, but the solution was not optically clear at a pH ≈ 5−7, possibly due to interparticle hydrogen bonding between the carboxyl functions of the ligands. To remove excess MPA from the supernatant solution, these particles were separated by centrifugation and decantation. Successive redispersion of the particles into water at pH = 10.8 yielded a clear solution.

Optical Characterization. UV−vis absorption spectra were taken with an Omega-10 spectrometer (Bruins Instruments), and photoluminescence (PL) spectra were taken with a Fluoromax-II fluorometer (ISA). Fluorescence quantum yields were estimated by comparison of the fluorescence intensity with standard dye solutions with the same optical density at the excitation wavelength and similar fluorescence wavelength.[40]

Transmission Electron Microscopy (TEM). A Philips EM-420 transmission electron microscope operating at an acceleration voltage of 120 kV was used to analyze size, size distribution, and the structure of core/shell nanocrystals. All of the samples were purified by acetone precipitation from their chloroform or hexane solutions. The nanocrystals were deposited from diluted solutions onto copper grids with carbon support. The size distribution histograms for all of the samples were obtained by analyzing more than 200 nanocrystals in each sample.

Energy-Dispersive X-ray Spectroscopy (EDX). For elemental analysis, a Tecnai F30ST (FEI) with a field emission gun operated at 300 kV equipped with an EDAX spectrometer with a Si/Li detector

(37) Schmelz, O.; Mews, A.; Basche, T.; Herrmann, A.; Mullen, K. *Langmuir* **2001**, *17*, 2861−2865.
(38) Yu, W. W.; Qu, L. H.; Guo, W. Z.; Peng, X. G. *Chem. Mater.* **2003**, *15*, 2854−2860.
(39) Wang, W. Z.; Germanenko, I.; El-Shall, M. S. *Chem. Mater.* **2002**, *14*, 3028−3033.
(40) Koberling, F.; Kolb, U.; Philipp, G.; Potapova, I.; Basche, T.; Mews, A. *J. Phys. Chem. B* **2003**, *107*, 7463−7471.

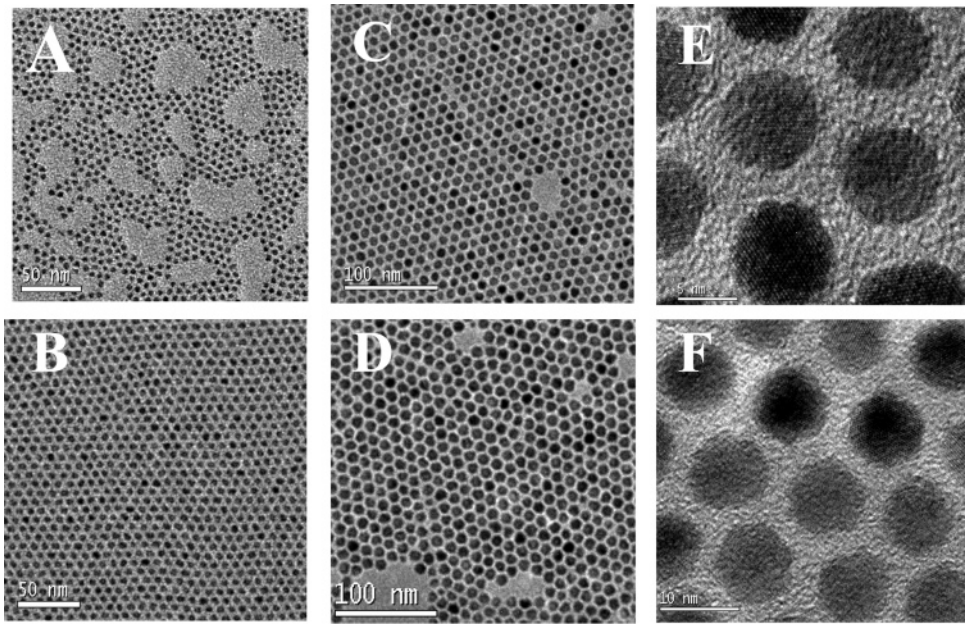

Figure 2. TEM images of the plain CdSe-cores and core/shell nanocrystals obtained under typical reaction conditions: (A) TEM images of CdSe-cores (before injection of Cd^{2+} solution); (B) (A) plus 2 monolayers of CdS; (C)/(E) (B) plus 3.5 monolayers of $Zn_{0.5}Cd_{0.5}S$; (D)/(F) (C) plus 2 monolayers of ZnS.

and an ultrathin window was used. The analysis was performed in the scanning mode with a beam diameter of ~1 nm at room temperature.

Powder X-ray Diffraction (XRD). Wide-angle X-ray diffraction (WAXS) was performed with a Siemens θ--θ diffractometer (D500T) in reflection geometry using Cu Kα radiation from a Siemens generator (Kristalloflex 710 H) operating at 35 kV and 30 mA, and a graphite monochromator. Measurements were performed in a 2θ range from 18° to 70°.

Photochemical and Colloidal Stability. The photo-oxidation experiments were performed under constant oxygen flow and irradiation from an HBO-50 ultraviolet lamp. UV−vis and PL-spectra were measured at certain time intervals after readjustment of the total volume of the QD-solution. The changes of the OD and normalized PL were used as indicators of the degradation of the nanocrystals dissolved in water and chloroform, respectively. The colloidal stabilities of nanocrystals were studied by repeated precipitation upon addition of methanol and successive redispersion in chloroform until the precipitate could not be dissolved anymore.

Results and Discussion

Reaction Conditions for Shell Growth of Different Compounds by SILAR. To conduct a comparative study of different shell materials, the core/shell CdSe/CdS/$Zn_{0.5}Cd_{0.5}S$/ZnS nanocrystals and several other core/shell systems including CdSe/CdS, CdSe/$Zn_{0.5}Cd_{0.5}S$, and CdSe/ZnS were synthesized from the same CdSe-cores with a similar overall shell thickness by using the SILAR method. In general, it was found that the reaction temperature greatly affects the growth of the shell in a way that seems to be different for various shell materials. For example, at high temperature, the reaction of the shell material might lead to the nucleation and subsequent formation of particles rather than to epitaxial growth of the shell.[33] However, using the SILAR approach, the amount of precursor needed to grow consecutive shells can be precisely calculated and the theoretical diameter of the particles after shell growth can be compared to the real diameters from TEM (see also Figure 3). For the growth of a CdS-shell, Peng et al.[33] demonstrated that at an optimum temperature of 240 °C the CdS was growing almost exclusively onto the CdSe cores resulting in nanocrystals

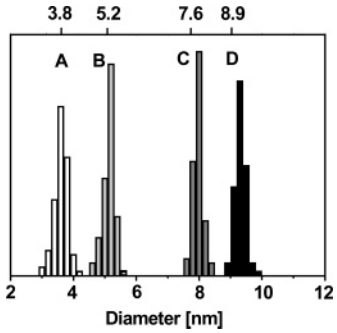

Figure 3. Size histograms for the series of samples shown in Figure 2. To build the histograms, the longest dimension for over 200 particles in each sample has been measured: (A) Histogram of CdSe-cores; (B) (A) plus 2 monolayer CdS; (C) (B) plus 3.5 monolayer $Zn_{0.5}Cd_{0.5}S$; (D) (C) plus 2 monolayer ZnS. The numbers on top mark the "theoretical" values for the expected diameters from geometric considerations.

with a narrow size distribution and a PL quantum yield (QY) of more than 40%.

To optimize the ZnS shell growth around the CdSe nanocrystals by SILAR using ZnO and S precursors, the reaction temperature was varied from 200 to 260 °C. At lower temperature, we found that the ZnS material did not grow completely onto the CdSe-cores, because no red-shift of the UV−vis and PL-peak but a strong additional absorption in the UV-range was observed. The experimental results indicated that the maximum QY of about 50% could be achieved if the growth of the ZnS shell took place at 245 °C. Therefore, the SILAR growth of ZnS and CdS using CdO, ZnO, and S precursors can be performed at a reaction temperature of 245 °C. Consequently, the different concentric shells were all grown under the same experimental conditions independent of the particular shell material.

Structural Characterization. We used several techniques to monitor the shell growth and characterize the structure, crystallinity, and composition of the prepared particles. Figure 2 shows TEM images of the CdSe-core nanocrystals and several core/shell nanocrystals with different shell thicknesses. In

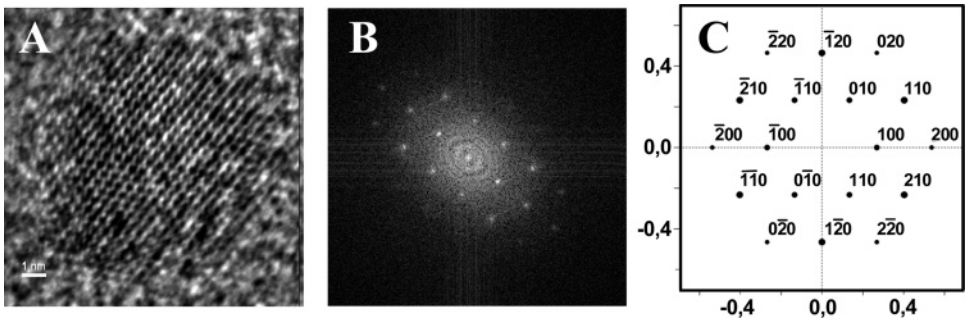

Figure 4. (A) HRTEM image of a CdSe/CdS/$Zn_{0.5}Cd_{0.5}S$/ZnS nanocrystal demonstrating its high crystallinity. (B) Fast-Fourier transform of the TEM image ($d_{FT(100)} = 3.77$ Å) shown in (A), which corresponds to the simulated diffraction pattern of the [001] crystal face of a wurzite CdSe particle ($d_{calc(001)} = 3.724$ Å) (C).

particular, the images show the core-CdSe nanocrystals after annealing at 240 °C for 10 min (A). The annealing process was necessary because the CdSe particles were slightly elongated after the growth process as described in the Experimental Section (see Supporting Information). Image B shows particles after growth of 2 MLs CdS, images C and E display the core/shell sample with 5.5 MLs (2 MLs CdS and 3.5 MLs $Zn_{0.5}Cd_{0.5}S$), and finally (D) and (F) show the core/shell sample with a coverage of 7.5 MLs (2 MLs CdS, 3.5 MLs $Zn_{0.5}Cd_{0.5}S$, and 2 MLs ZnS).

The size histograms of the same nanocrystals as in Figure 2 are shown in Figure 3. We determined a mean diameter of 3.8 ± 0.30 nm for the bare CdSe-cores, which increases to 5.3 ± 0.25 nm after coverage with 2 MLs of CdS. The coverage with 3.5 MLs of $Zn_{0.5}Cd_{0.5}S$ leads to a diameter of 7.9 ± 0.28 nm, which finally is increased to 9.2 ± 0.34 nm upon coverage with the outermost shell of 2 MLs ZnS to form the final core/shell NCs with 7.5 MLs of shell material (2 MLs CdS/3.5 MLs $Zn_xCd_{1-x}S$/2 MLs ZnS). Obviously, the size distribution is narrow even though the particles are coated with 7.5 MLs of shell material as shown in Figure 3.

A HRTEM image of a single CdSe/CdS/$Zn_{0.5}Cd_{0.5}S$/ZnS nanocrystal is given in Figure 4A. Similarly to most of the particles, the TEM image of this nanocrystal reveals a high crystallinity with continuous lattice fringes throughout the whole particle. This particular particle is viewed along the crystallographic *c*-direction. Correspondingly, the Fourier transform of the image shown in Figure 4B is in almost perfect agreement with the calculated diffraction pattern of the CdSe wurzite structure, aligned along the [001] crystal face direction (Figure 4C). The blurry appearance at the rim of this particle (Figure 4A) might be due to the molecular ligands.

We also performed TEM measurements of other core/shell samples, which have been synthesized for comparison (see Supporting Information). For the CdSe/6ML CdS core shell particles, we could reproduce the results of Peng et al.[33] and found a size distribution of 7.3 ± 0.43 nm, which is comparable to the size distributions of the complex shells shown in Figures 2 and 3. On the other hand, the size distributions for the CdSe/ZnS particles were much broader. Here, we measured distributions of 7.1 ± 2.2 nm using the traditional method and 7.2 ± 0.98 nm using the SILAR method. Importantly, we found that the CdSe/ZnS core/shell nanoparticles synthesized by both methods also showed a larger number of lattice defects and irregular shapes. This shows that the "imperfect growth", which is obtained for thick ZnS-shells,[27] is not due to the preparation

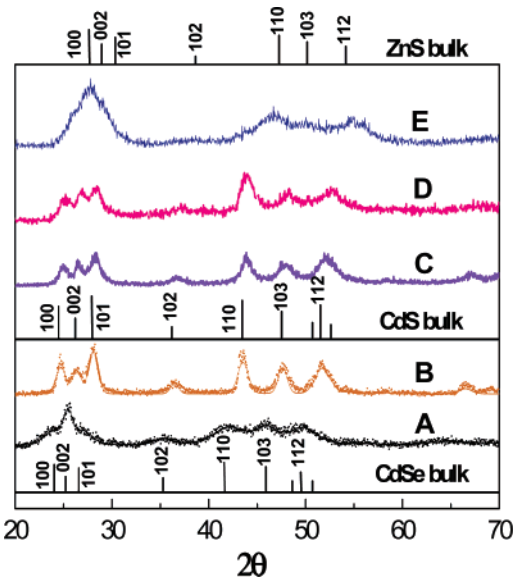

Figure 5. Powder XRD patterns of the different samples: (A) CdSe NCs, (B) CdSe + 6 MLs CdS NCs, (C) CdSe + 6 MLs $Zn_{0.5}Cd_{0.5}S$ NCs, (D) CdSe/2 MLs CdS/2 MLs $Zn_{0.5}Cd_{0.5}S$/2 MLs ZnS NCs, and (E) CdSe/6 MLs ZnS NCs.

method but rather related to the large difference in lattice parameters between CdSe and ZnS.

To identify the core/shell structure, we also investigated the crystallographic properties by powder X-ray diffraction (XRD). Figure 5 compares the XRD patterns of several samples to the theoretical peak positions of the wurzite bulk materials of CdSe,[41] CdS,[42] and ZnS,[43] respectively. The powder XRD pattern of the CdSe-cores (A) results form the elongated CdSe cores before annealing and can be compared to the TEM image (A) in the Supporting Information. Basically, the peak positions match the theoretical values of the wurzite structure of CdSe.[44] The peak broadening is due to the reduced size of the particles.[16] The solid line is a result of a particle size analysis based on a Pawley-fit[44] and using Scherrer's formula,[45] which is consistent with particle dimensions of 3.2 nm across the crystallographic *a*- and *b*-directions and 5.8 nm along the *c*-direction and therefore in agreement with the TEM results presented in the Supporting Information.

(41) Stevenson, A. W.; Barnea, Z. *Acta Crystallogr., Sect. B* **1984**, *40*, 530−537.
(42) Yeh, C.; Lu, Z. W.; Froyen, S.; Zunger, A. *Phys. Rev. B* **1992**, *46*, 10086−10097.
(43) Saliba, S.; Mardix, S. *Acta Crystallogr., Sect. A* **1983**, *39*, 933−936.
(44) Scientific software Cerius^2, 4.2ms ed.; Accelrys Inc.: San Diego, CA.
(45) Scherrer, P. *Gött. Nachr.* **1918**, *2*, 98.

The diffraction patterns shown in Figure 5B−E result from particles synthesized from the annealed core particles (image B in the Supporting Information), which were covered with 6 MLs each of different shell materials. Sample B is covered with 6 MLs of CdS, sample C with 6 MLs of the $Zn_{0.5}Cd_{0.5}S$-alloy, sample D with 2 MLs CdS/2 MLs $Zn_{0.5}CdS_{0.5}S$/2 MLs ZnS, and finally sample E with 6 MLs of ZnS. For all of the core/shell particles, the volume fraction of the cores is less than 10% of the total volume. Therefore, the XRD peak positions are much closer to the corresponding values of the shell bulk material than to the CdSe-core material. For example, the peak positions of curve B are close to the values of CdS and the peak widths are much narrower as a result of the larger particle diameter. For samples C (Cd/ZnS-alloy shell) and D (multilayer shell), the peak positions are slightly shifted toward the bulk values of ZnS, because of the increasing amount of ZnS. Actually, the outmost 2 MLs of ZnS in sample D have a volume fraction of about 30%, but the peak width remains relatively narrow. In contrast, the peak positions of sample E, where the CdSe cores were covered with 6 MLs of ZnS, are close to the ZnS values, and the peak widths are broad.

While a more detailed analysis of the diffraction patterns from the core/shell particles is desirable, several qualitative arguments can be raised from the data at hand. First, especially the CdS material seems to grow without the formation of lattice defects, because the peak widths are narrow. In a first approximation, we fitted the diffraction pattern of sample B with the same procedure as mentioned above[44] and obtained the hexagonal lattice parameters $a = b = 0.4156$ nm and $c = 0.675$ nm. These values are much closer to CdS ($a = b = 0.412$ nm, $c = 0.668$ nm) than to CdSe ($a = b = 0.430$ nm, $c = 0.701$ nm). In sample E, where the shell consists of ZnS only, the broad diffraction peaks go along with a broad diameter distribution and irregular particle shapes as observed by TEM. Obviously, the large lattice mismatch between CdSe and ZnS leads to an imperfect shell growth and a short coherence length of the diffracted X-rays, which in turn results in broad diffraction peaks. The diffraction patterns of samples C and D appear to be similar to each other and much different from sample E. Therefore, we assume that even though the volume fraction of ZnS is relatively high (35% in sample C and even 58% in sample D), the shell growth still happens in an epitaxial manner, because the stress can be released in the radial direction.

To further identify the chemical composition of the particles, we used EDX spectroscopy in parallel and scanning mode. The analysis has been performed with the Cd−L, Zn−L, S−K, and Se−L lines with the elements C, O, Cu, and Si included in the background. To avoid the effects of drift and to reduce the contamination of the sample during measurement, we did not investigate a single particle but 5−10 particles in parallel. Figure 6 shows the EDX spectrum of seven particles where the CdSe-cores were covered with a shell composition of 2 MLs CdS, 3.5 MLs $Zn_{0.5}Cd_{0.5}S$, and 2 MLs ZnS. It can be seen that the Se bands are almost completely hidden by the background signal, while the other elemental bands can clearly be resolved. However, a quantitative analysis results in a composition of $Cd_{20}Zn_{30}Se_5S_{45}$ for the seven selected multishell particles investigated. This needs to be compared to the elemental distribution as calculated for an "ideal" core shell particle, which would have the stoichiometry of $Cd_{25}Zn_{28}Se_4S_{43}$. The correspondence of the theoretical and experimental values suggests that the individual particles have the composition assumed and that no separated ZnS and/or CdS particles have been formed during the shell growth.

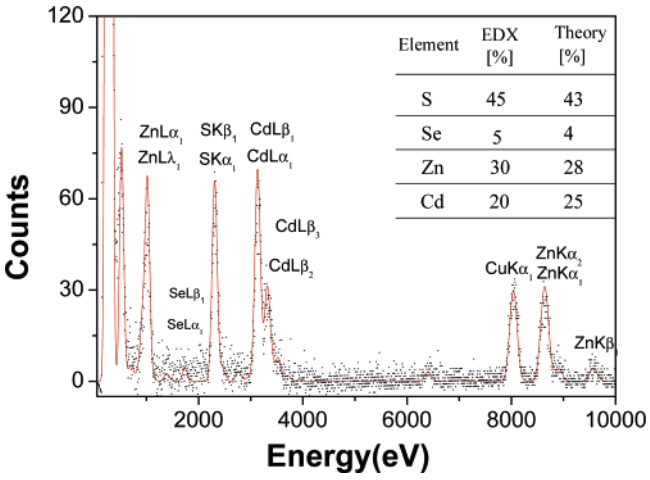

Figure 6. EDX spectrum of an array of seven particles of CdSe-core (2 MLs CdS/3.5 MLs $Zn_{0.5}Cd_{0.5}S$/2 MLs ZnS)−shell NCs prepared on a copper grid. The inset illustrates the comparison of theoretical and experimental values.

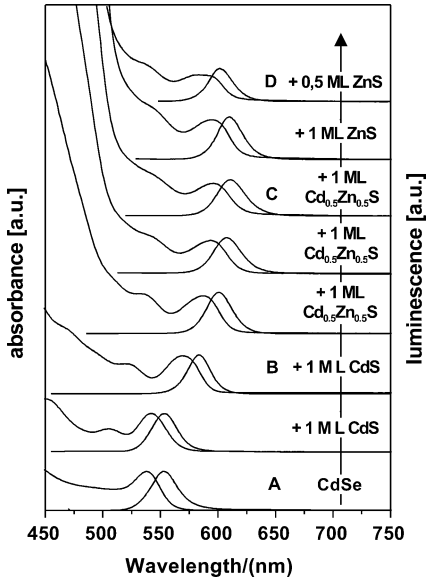

Figure 7. Evolution of the absorption and photoluminescence spectra upon consecutive growth of the concentric shells. The spectra labeled with the letters A−D were taken from the same samples, which led to the TEM pictures A−D in Figure 2 and the corresponding size distributions in Figure 3.

Optical Characterization. The UV−vis and PL-spectra of the core/shell nanocrystals from a typical reaction are shown in Figure 7. The spectra labeled with the letters A−D were taken from the same samples that led to the TEM pictures A−D in Figure 2. It can be seen that during the shell growth, the absorption and PL-spectra shift to the red due to the larger extension of the electronic wave function leaking out into the shell material.[46] At the same time, the spectra maintain their overall shape, which is consistent with the narrow size distributions of the core/shell nanocrystals shown in Figure 3. A closer look reveals that the absorption and PL-spectra show slight blue-

(46) Schoos, D.; Mews, A.; Eychmüller, A.; Weller, H. *Phys. Rev. B* **1994**, *49*, 17072−17078.

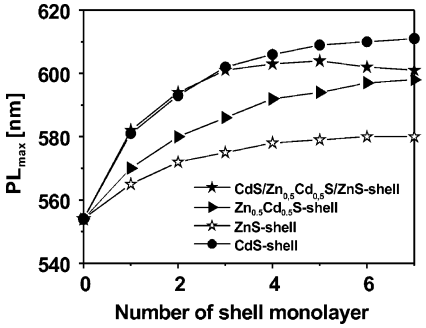

Figure 8. Evolution of the PL-peak position for several core/shell particles. The PL-band shifts toward longer wavelength upon shell growth on the CdSe-cores due to the decrease in confinement. The multishell particles show a slight blue-shift upon growth of the outer ZnS layers.

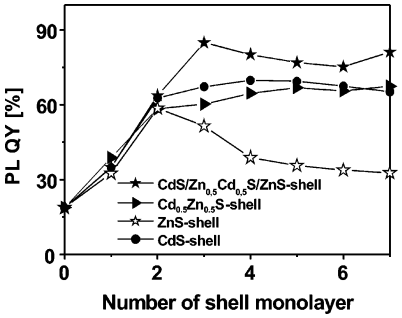

Figure 9. Evolution of the photoluminescence quantum yield for several core/shell particles. The QY is increasing upon shell growth due to the electronic passivation of the surface. For the CdSe/ZnS core/shell particles, the QY decreases for shell thicknesses larger than 2 MLs, probably due to lattice imperfections within the shell.

Table 1. Photoluminescence Quantum Yield of Core and Core/Shell Nanocrystals Covered with ODA in Chloroform As Compared to the MPA-Covered Particles in Water

	photoluminescence quantum yield			
ligand/solvent	CdSe core	CdSe/CdS core/shell	CdSe/ZnS core/shell	CdSe/CdS/ZnCdS/ZnS core/multishell
ODA/chloroform	0.3	0.51	0.41	0.7
MPA/water	≪0.01	0.11	0.25	0.48

shifts when the outer layers of ZnS were coated onto the CdSe/CdS/Zn$_{0.5}$Cd$_{0.5}$S core/shell nanocrystals. This blue-shift became obvious when the solution was kept for 30 min at 260 °C (Figure 7D). A blue-shift was also observed when CdSe-nanorods were covered with a composite CdS/ZnS-shell and annealed by laser irradiation.[32] The authors attributed this effect to partial photodegradation of the CdSe cores. Because the blue-shift observed in this work happens only if the particles are covered with additional ZnS, we think that the reason for this spectral shift is the partial formation of a Zn$_x$Cd$_{1-x}$S alloy shell. Especially at high temperature the Zn-atoms might diffuse into the Cd-rich regions of the shell, thus increasing the band-offset of the shell and hence the effective confinement.[35,47]

To verify this assumption, we compared the evolution of the PL-position upon growth of the CdSe/CdS/Zn$_{0.5}$Cd$_{0.5}$S/ZnS core/shell nanocrystals with other core/shell nanocrystals, including CdSe/CdS, CdSe/Zn$_{0.5}$Cd$_{0.5}$S, and CdSe/ZnS. The particles were prepared from the same batch of CdSe-cores. The SILAR method allowed one to grow the same number of monolayers of each shell. As can be seen in Figure 8, the red-shift for the CdSe/CdS particles (55 nm) is much more pronounced than that for the CdSe/ZnS core/shell nanocrystals (25 nm), while the evolution of the position of the PL-band from the CdSe/Zn$_{0.5}$Cd$_{0.5}$S alloy shell lies qualitatively in between. For the CdSe/CdS/Zn$_{0.5}$Cd$_{0.5}$S/ZnS multishell structure, one can see that initially it follows the graph of the CdSe/CdS particles, because the first two MLs consist of CdS. The position of the PL-band is then almost constant upon growth of three layers of the Zn$_{0.5}$Cd$_{0.5}$S alloy but is slightly blue-shifted upon the final growth of the outermost 2 MLs of ZnS. Obviously, the final position of the PL-band is similar to that of the CdSe/Zn$_{0.5}$Cd$_{0.5}$S particles with alloyed shell. However, because the outermost shell comprised a higher volume fraction, the CdS/Zn$_{0.5}$Cd$_{0.5}$S/ZnS shell contains 65% ZnS and only 35% CdS, in contrast to the purely alloyed shell, where the volume fractions are equal. Therefore, we assume that the interdiffusion effect that causes the blue-shift mainly happens at the interface between CdS and ZnS and that the outer surfaces of the CdSe/CdS/Zn$_{0.5}$Cd$_{0.5}$S/ZnS multishell particles are still ZnS-rich, which could also explain the "chemical effects" discussed below.

The PL-QY of the same core/shell nanocrystals is shown in Figure 9. While the QY of the plain CdSe-core particles is of the order of 20%, it can increase to about 60% upon coverage of two MLs of ZnS, CdS, or Zn$_{0.5}$Cd$_{0.5}$S by SILAR, independent of the shell material. Additional growth of ZnS shells leads to a reproducible decrease in the QY, which is in agreement with former experiments, where the ZnS shell was grown by the "traditional method".[27] This suggests that the formation of defects upon the growth of relative thick ZnS-shells, which is supposed to be the reason for the decrease in the QY, is not due to the growth process but indeed a result of the accumulated lattice strain. In contrast, the QY for the particles with CdS-shell, Zn$_{0.5}$Cd$_{0.5}$S-shell, or CdS/Zn$_{0.5}$Cd$_{0.5}$S/ZnS-multiple shell is even slightly increasing upon further shell growth. While the absolute values were slightly different from batch to batch, we could reproducibly observe that the final QYs of the particles with the CdS- and Zn$_{0.5}$Cd$_{0.5}$S-shells were in the range of 65%, while coverage with the CdS/Zn$_{0.5}$Cd$_{0.5}$S/ZnS-multishell yielded a slightly higher QY of about 80%.

PL-Response upon Chemical Surface Modification. To investigate the influence of molecular surface modification on the PL-QY for the different core/shell particles, we performed several ligand exchange experiments. In particular, we measured the PL of amine-covered core/shell particles and compared it to the PL after ligand exchange with thiols, as explained in the Experimental Section. As a thiol, we picked mercapto propionic acid (MPA), because the ligand exchange leads to a change of the surface polarity from hydrophobic to hydrophilic.[13] Hence, the particles, which were initially soluble in chloroform, become water soluble and the ligand exchange could be followed by the change of solubility.

In Table 1, we compare the PL-QY of (TOPO)/ODA-covered CdSe-cores and different ODA-covered core/shell nanocrystals in chloroform, with the PL-QY of the same MPA-covered particles in water. We found that the MPA coating of the CdSe cores leads to a nearly complete quenching of the PL, consistent with earlier observations.[33] In contrast, the PL of the core/shell nanocrystals was only partially quenched after ligand exchange by the thiols. However, the decrease of the PL-QY depends on

(47) Zhong, X. H.; Han, M. Y.; Dong, Z. L.; White, T. J.; Knoll, W. *J. Am. Chem. Soc.* **2003**, *125*, 8589−8594.

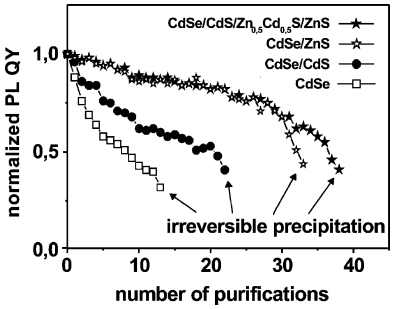

Figure 10. Evolution of the relative photoluminescence quantum yield upon repeated precipitation and redispersion of TOPO/ODA-covered CdSe cores and several ODA-covered core/shell particles in chloroform solution. The relative QY and the colloidal stability are higher for particles with an outer shell of ZnS.

the particular core/shell nanocrystals. We found that the PL is decreasing to a stronger degree for particles with a CdS-shell. This is most likely due to the smaller band offset for the CdSe/CdS material combination (see Figure 1), which leads to a higher probability for the charge carriers to be found at the particle surface. While the relative decrease of the PL-QY is similar for the CdSe/ZnS- and CdSe/CdS/$Zn_{0.5}Cd_{0.5}$S/ZnS-nanocrystals, the absolute QY of the MPA-coated multishell particles is still of the order of 50%, due to the higher initial QY of those particles.

In the following experiments, we compare the relative QYs of different nanocrystals and focus on ODA-covered particles. In general, it was shown that the high QY of amine-covered particles[19] can only be observed in solutions with excess of ligands,[48,49] probably because of a dynamic exchange equilibrium between ligands on the surface and in solution.[37] In addition, it was observed that the amines are more strongly bound to the CdSe/CdS particles than to the plain CdSe cores.[33] Here, we investigated the "colloidal stability" in detail by performing repeated precipitation of the particles and successive redispersion in pure solvents. From Figure 10, it can be seen that the PL-QY of the CdSe cores, which were prepared in a 1:1 mixture of TOPO/ODA, indeed drops fast upon repeated precipitiation by addition of methanol and redispersion into chloroform, until the particles cannot be redissolved anymore after about 10 purification cycles. Under the same conditions, the CdS-covered particles could be purified more than 20 times before they became insoluble, which is consisted with earlier observations.[33] However, if the outer surface shell of the NCs consists of ZnS, the "colloidal stability" was even higher and the CdSe/ZnS particles as well as the CdSe/CdS/$Zn_{0.5}Cd_{0.5}$S/ZnS-multishell particles could be purified more than 30 times before they became insoluble. This suggests that the amines are more strongly bound to Zn-sites on the surface of the nanocrystals than to Cd-sites. By comparing fluorescence intensities of the particles with an outer ZnS layer, it should be noted that the absolute PL-QY of the multishell particles is still of the order of 25% before irreversible precipitation, while the QY of the CdSe/ZnS core shell particles is only 10−15%.

Another important issue especially for the use of semiconductor nanocrystals in optical applications is the evolution of the optical properties under continuous irradiation. In this context,

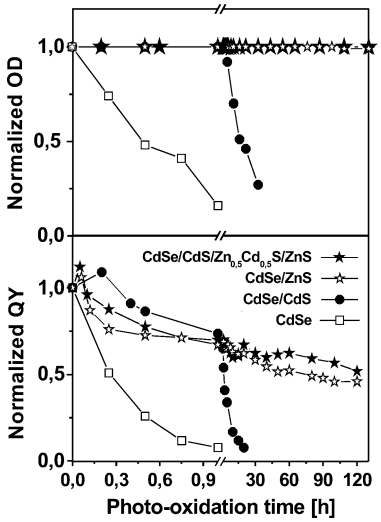

Figure 11. Photochemical stability of nanocrystals in oxygen saturated chloroform solutions under UV-irradiation. (top) Change in optical density and (bottom) change in photoluminescence quantum yield for the CdSe-core and different core shell particles (for details, see text).

it is often observed that nanocrystals degrade in time due to photo-oxidatation.[18] Figure 11 shows the change of the optical density (top) and relative fluorescence intensity (bottom) upon irradiation of oxygen saturated solutions of the different nanoparticles in chloroform, as described in the Experimental Section. It can be seen that the absorption of the CdSe particles drops rapidly and the particles precipitate after a period of 1.5 h. The "stability" of the particles can be increased by overcoating with CdS, as has been shown already.[25] The nanocrystals with a topmost layer of ZnS were even more stable, and the optical density changed only slightly until the particles precipitated from solution, that is, after 12 days for the particles with the pure ZnS-shell and 10 days for the multishell particles.

While studying the PL properties of the nanocrystals under photo-oxidation conditions (Figure 11, bottom), a brightening phenomenon was observed in the first minutes for most of the particles.[50] At longer times, the PL QY of all samples investigated decreased little by little, most likely as a result of photo-oxidation on the surface. In general, we could observe a trend similar to that for the change of the absorption spectra. The fluorescence of CdSe nanocrystals decreased fast and was associated with a blue-shift of the fluorescence band position from 570 to 510 nm, which is attributed to a shrinking of the CdSe core. The fluorescence intensity of the CdSe/CdS core shell particles decreased to a lower degree initially, and we could also observe a shift of the fluorescence band, in this case from 620 to 610 nm. In contrast, a shift of the fluorescence band could not be observed either for the CdSe/ZnS particles or for the multishell particles. At the same time, the fluorescence intensities of those samples decreased only by approximately 50% upon illumination for more than 120 h.

Obviously, the particles with an outer layer of ZnS show a much higher photochemical stability. This is most likely due the higher band offset introduced by the ZnS material as compared to CdS, which results in a lower charge density of the photogenerated charge carriers on the particle surface and hence a lower probability of surface oxidation. Therefore, the

(48) Qu, L.; Peng, X. *J. Am. Chem. Soc.* **2002**, *124*, 2049−2055.
(49) Potapova, I.; Mruk, R.; Prehl, S.; Zentel, R.; Basche, T.; Mews, A. *J. Am. Chem. Soc.* **2003**, *125*, 320−321.
(50) Nazzal, A. Y.; Wang, X. Y.; Qu, L. H.; Yu, W.; Wang, Y. J.; Peng, X. G.; Xiao, M. *J. Phys. Chem. B* **2004**, *108*, 5507−5515.

particles with an outer layer of ZnS show a higher chemical stability and also a higher long-term fluorescence intensity.

Conclusion

We have presented a detailed comparative study of core−shell nanocrystals, where the surface of CdSe cores was passivated by the shell materials ZnS and CdS or a combination of these materials. While the shell material ZnS leads to a suitable electronic passivation due to the large band offsets with respect to CdSe, the CdSe/ZnS core shell particles are irregular in shape and the fluorescence quantum yield decreases for large shell thicknesses due to lattice imperfections. The shell material CdS, on the other hand, can grow in an almost epitaxial manner due to the small lattice mismatch, but the electronic passivation is less effective because of relatively low band offsets. To overcome these problems, we have used the newly developed SILAR technique to gradually change the shell composition in the radial direction from CdS to ZnS. In this way, the lattice strain can relax in the radial direction and the particles show a high crystallinity, similar to pure CdS shell material. At the same time, the band offsets are quite high and the particles are well electronically passivated, similar to pure ZnS-shell materials. This shows that the passivation shell of semiconductor nanocrystals can now be engineered in a defined way, leading to particles with high crystallinity, well-defined electronic structures, and distinct chemical surface properties.

Acknowledgment. This work was supported by a grant from the SFB 625 (B7).

Note Added in Proof: During the reviewing process, a paper on a similar topic was published by Talapin et al.[51]

Supporting Information Available: TEM images of different nanocrystals. This material is available free of charge via the Internet at http://pubs.acs.org.

JA042939G

(51) Talapin, D. V.; Mekis, I.; Gotzinger, S.; Kornowski, A.; Benson, O.; Weller, H. *J. Phys. Chem. B* **2004**, *108*, 18826−18831.